HIGH SPEED FLOW OVER A FLAT PLATE AND ON A STEP OBSTACLE

Paulo G. P. Toro
e-mail: toro@ieav.cta.br
Francisco D. Rocamora Jr.
e-mail: junior@ieav.cta.br
Mauricio A. Pinheiro Rosa
e-mail: pinheiro@ieav.cta.br
Marco A. Sala Minucci
e-mail: sala@ieav.cta.br

Instituto de Estudos Avançados - IEAv/CTA
Rod. Dos Tamoios, Km 5,5
12.231-970 - São José dos Campos - SP, Brasil

Abstract. *Hypersonic flow over a flat plate and on a step obstacle are investigated using the explicit finite difference MacCormack's time marching technique. The complete Navier-Stokes equations are treated in a 2D geometry and the shock wave and viscous boundary layer are examined for different boundary conditions. Air is considered a calorically perfect gas with constant Prandtl number and Sutherland's law is used for the viscosity. The results include pressure, velocity and temperature profiles on the wall and at the trailing edge as well as 2D contours for different Mach numbers.*

Keywords*: Hypersonic Flow, Numerical Methods, Boundary Layer, Shock Wave, Flat Plate, Step Obstacle.*

1. Introduction

Currently a numerical group on aerothermodynamics of hypersonic flows is being formed at the IEAv/CTA, aiming at giving theoretical support through the use of numerical methods to the already well established experimental group. This work represents the initial step towards accomplishing this objective. Two simple supersonic and hypersonic flow problems are dealt with and some results are commented upon. The problems are: *a*) hypersonic flow over a flat plate and, *b*) supersonic and hypersonic flow over a step obstacle. The flat plate problem has already been investigated by many authors as, *e.g.*, Anderson (1989) Anderson (1990), Anderson (1995), Toro *et al*. (1998), Nagamatsu *et al*. (1994), Moraes *et al*. (1991). These problems were chosen due to the different nature of the shock waves that appear in these two geometries. In the former one, the flat plate, the shock wave starts on the plate's front tip and is due to the formation of a boundary layer over the plate, *i.e.*, viscous effects, such that the shock is oblique. In the later, the step obstacle, a detached shock wave is formed due to the bluntness of the obstacle, and, differently from the flat plate case, the shock is almost normal.

A computer program in FORTRAN language was developed, using the shock capturing MacCormack's technique, in order to solve numerically the proposed problems. It should be emphasized that the models implemented in this program do not take in to account hypersonic effects on the fluid, such as, vibrational excitation, molecular dissociation, etc.

2. Flow geometry

The flow geometries for the two problems studied in this work are shown in Fig.1 together with the domains used for the numerical calculations. For both geometries the flow enters the domain from the left boundary and leaves at the right boundary so that the free stream boundary condition is always imposed on the left boundary. In the Flat Plate case, Fig. 1 *a*), the free stream condition is imposed on the upper boundary and the lower boundary is an impermeable wall over which the boundary layer and the shock wave develop. In the Obstacle case, the free stream condition is also imposed on the upper boundary and there are two possible conditions for the lower boundary, *i.e.*, symmetry at the obstacle midplane using half of the domain or, as shown in Fig. 1 *b*), free stream condition considering the obstacle midplane in the middle of the domain.

3. Mathematical model

For a 2D compressible flow, the complete Navier-Stokes' equations in the conservative form can be written as [Anderson (1995)]:

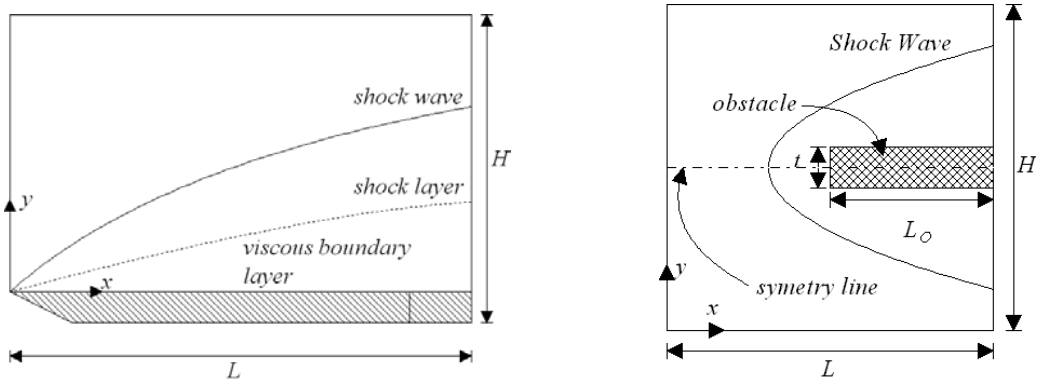

a) *b*)

Figure 1. Flat Plate and Obstacle Geometries.

- Continuity equation:

$$\frac{\partial \rho}{\partial t}+\frac{\partial}{\partial x}(\rho u)+\frac{\partial}{\partial y}(\rho v)=0 \tag{1}$$

- Momentum equations:

- *x* direction -

$$\frac{\partial}{\partial t}(\rho u)+\frac{\partial}{\partial x}(\rho u^2+p-\tau_{xx})+\frac{\partial}{\partial y}(\rho u v-\tau_{yx})=0 \tag{2}$$

- *y* direction -

$$\frac{\partial}{\partial t}(\rho v)+\frac{\partial}{\partial x}(\rho u v-\tau_{xy})+\frac{\partial}{\partial y}(\rho v^2+p-\tau_{yy})=0 \tag{3}$$

- Energy equation:

$$\frac{\partial}{\partial t}(E_t)+\frac{\partial}{\partial x}\left[(E_t+p)u+q_x-u\tau_{xx}-v\tau_{xy}\right]+\frac{\partial}{\partial y}\left[(E_t+p)v+q_y-v\tau_{yx}-v\tau_{yy}\right]=0 \tag{4}$$

where E_t in the above equation is the total energy, *i.e.*, the sum of the kinetic energy plus the internal energy , e ,per unit volume, defined as:

$$E_t=\rho\left(e+\frac{V^2}{2}\right) \tag{5}$$

The normal and shear stress, in terms of velocity gradients, are given as:

$$\tau_{xx}=\lambda(\nabla\cdot\mathbf{V})+2\mu\frac{\partial u}{\partial x} \tag{6}$$

$$\tau_{yy}=\lambda(\nabla\cdot\mathbf{V})+2\mu\frac{\partial v}{\partial y} \tag{7}$$

$$\tau_{xy}=\tau_{yx}=\mu\left(\frac{\partial u}{\partial y}+\frac{\partial v}{\partial x}\right) \tag{8}$$

The components of the heat flux vector appearing in Eq. (4) are given below:

$$q_x = -k\frac{\partial T}{\partial x} \tag{9}$$

$$q_y = -k\frac{\partial T}{\partial y} \tag{10}$$

In the above equations the symbols retain the usual meaning, i.e., x and y are the Cartesian coordinate system, ρ is the fluid density, u and v are the x and y components of the velocity vector $\mathbf{V}$ ($|\mathbf{V}| = V = \sqrt{x^2 + y^2}$), p is the pressure, μ is the molecular viscosity, λ is the second coefficient of viscosity, τ_{ij} ($i,j=x,y$) are the stress tensor components, q_i ($i=x,y$) are the heat flux components, T is the temperature and k is the thermal conductivity.

In order to close the system of equations given above, four additional equations are necessary, as given below:
- Perfect gas is assumed:

$$p = \rho R T \tag{11}$$

- Air is considered calorically perfect:

$$e = c_v T \tag{12}$$

- The viscosity is evaluated through Sutherland's law:

$$\mu = \mu_0 \frac{T^{3/2}}{T + 110} \tag{13}$$

where μ_0 is a reference value at sea level.
- Again, considering air as calorically perfect, the thermal conductivity can be obtained from the Prandtl number (which is approximately 0,71), as:

$$k = \frac{\mu c_p}{\mathrm{Pr}} \tag{14}$$

where c_p and c_v are the specific heats at constant pressure and constant volume, respectively.

4. Numerical method

In order to solve the partial differential equations (1) to (4) given in the previous section, the MacCormack's time marching scheme is utilized [Anderson (1995)]. This scheme uses 'forward' spatial differences for the prediction step and 'backward' spatial differences for the correction one. A computational program in FORTRAN language was developed which embodies all the characteristics necessary to deal with the proposed problems. Several uniform grids are used to assess solution accuracy. The grids were generated using the LevSoft (1998) software. The results are considered converged when the relative density variation reaches a specified accuracy in the entire domain. The boundary conditions are the ones described in section 2, with the sea level free stream conditions:

$$\begin{aligned} M &= M_0 \\ p &= p_0 \\ \rho &= \rho_0 \\ \mathbf{V} &= \mathbf{V}_0 \\ T &= T_0 \end{aligned} \tag{15}$$

5. Results and discussion

Several runs were made for both the flat plate and the obstacle problems. The results will be presented separately for clearness. Also, the values of the main parameters utilized for all the cases considered are given in Table 1.

Table 1. Main parameters considered.

p_0 (Pa)	T_0 (K)	μ_0 (N·s/m^2)	Pr	R (kg/J·K)	γ
101325.	288.16	$1.458 \cdot 10^{-6}$	0.71	287.	1.4

5.1. Flat plate results

For the flat plate problem, two different boundary conditions (BC's) were considered for the energy equation, *i.e.*, uniform temperature and adiabatic plate surface. The length of the plate utilized was $L = 10^{-5}$ m. Figures 2 to 5 below show some of the results obtained.

Figure 2 shows the influence of the mesh size on the pressure distribution over the flat plate surface. As can be seen, refining the mesh improves the results in the region near the front tip of the plate where pressure can reach very high values. For a uniform 70x70 grid, one finds negative values for the pressure, at least for one point, over the plate surface, which is not realistic. This indicates that care should be exercised in choosing a mesh size for a specific problem.

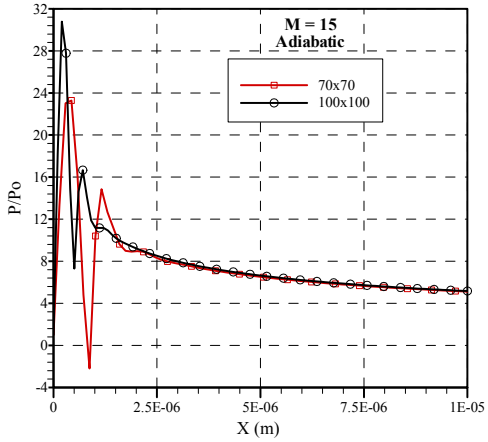

Figure 2. Pressure distribution on the flat plate surface for Mach number 15 and two meshes with adiabatic energy BC.

Next, temperature, pressure and Mach number profiles at the trailing edge of the plate for two Mach numbers and the two BC's considered are shown. Figures 3 *a*), *b*) and *c*) show the distributions for the uniform temperature BC and two Mach numbers, 4 and 15. Figures 4 *a*) and *b*) show the distributions for the two BC's and Mach number 4.

Figures 3 *a*) and 4 *a*) show that the pressure peaks occur right behind the shock in all the cases, while the maximum temperatures occur close to the plate surface or on it as seen from Figs. 3 *b*) and 4 *b*). One can also notice a significant increase in peak temperature and pressure as the Mach number increases. Also from Fig. 3 *a*) one can notice that the pressure variation through the boundary layer is basically uniform for low Mach numbers while its variation can not be neglected for hypersonic Mach numbers.

It should be mentioned that outside the boundary layer, the pressure variation normal to the plate surface in the shock layer region is very high.

Figure 3 *c*) shows the Mach number distributions at the trailing edge for two free stream Mach numbers, 4 and 15, and uniform temperature BC. From this figure one can observe the boundary layer thickness as compared to the shock layer. It also shows that the higher the Mach number the closer the two layers get. Also, as the Mach number increases, both layers lay down towards the plate surface.

Some of the results shown for the flat plate problem were confronted with the ones presented in Anderson (1995), Toro *et al*. (1998) and Moraes *et al*. (1991), comparing well.

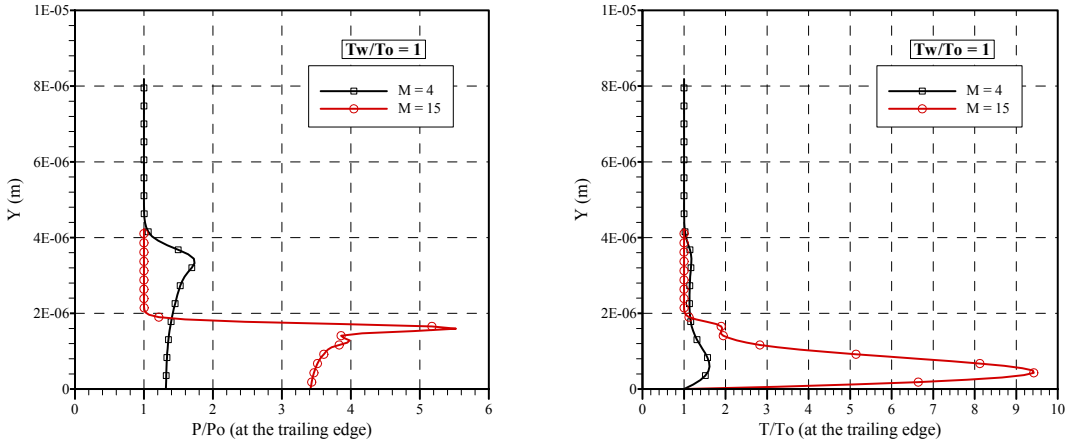

a) *b*)

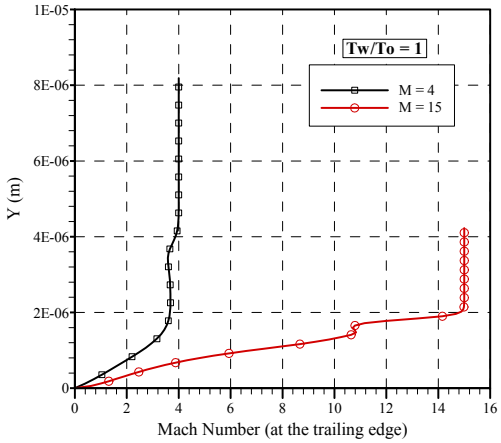

c)

Figure 3. Pressure, Temperature and Mach number distributions at the trailing edge for uniform temperature BC: *a*) Pressure, *b*) Temperature and *c*) Mach number.

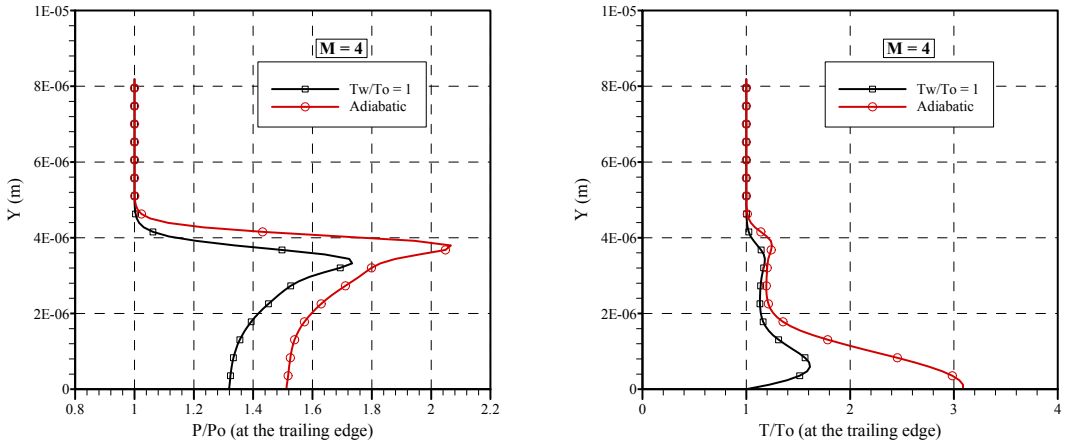

a) *b*)

Figure 4. Pressure and Temperature distributions at the trailing edge for Mach number 4 and two BC's: *a*) Pressure and *b*) Temperature.

Figures 5 *a*) and *b*) show contour plots for the temperature and Mach number for the case of Mach number 4 and adiabatic BC. As the shock over the flat plate is an oblique shock (due to the boundary layer formation), the Mach numbers behind the shock can be greater than 1, as can be seen in Fig. 5 *b*). Only very close to the plate surface, were the no-slip condition is imposed, the Mach number becomes smaller.

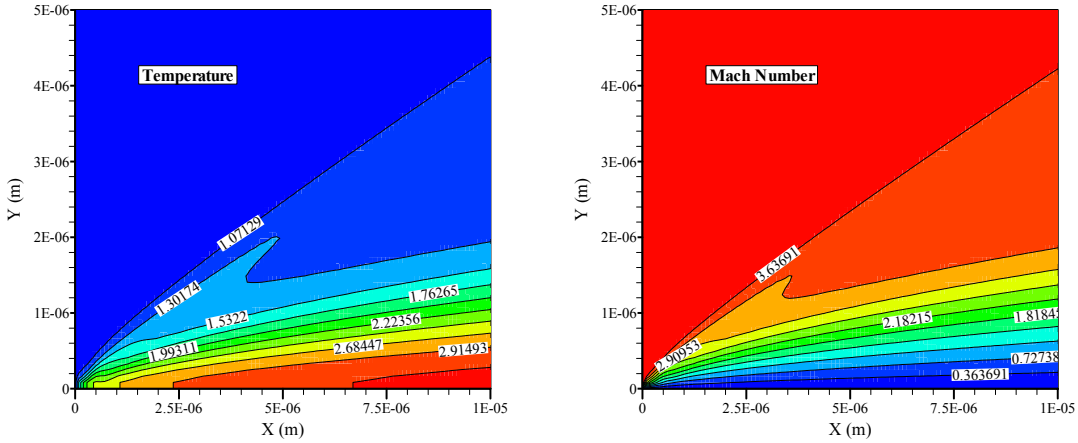

a) *b*)

Figure 5. Contour maps for Mach number 4.

5.2. Step obstacle results

For the step obstacle problem, the length of the obstacle considered was $L_o = 5 \cdot 10^{-6}$ m, and the thickness was $t = 2 \cdot 10^{-6}$ m. All the results shown here were obtained for the symmetry BC at the obstacle midplane and uniform temperature on the obstacle's surface ($T_w/T_0 = 1$). The results were obtained for three Mach numbers, 3, 4 and 8.

Figure 6 shows the pressure and temperature profiles along the obstacle's midplane. Along this line there is a normal shock so that the pressure and temperature rise abruptly across the shock, as expected, following closely the normal shock relations.

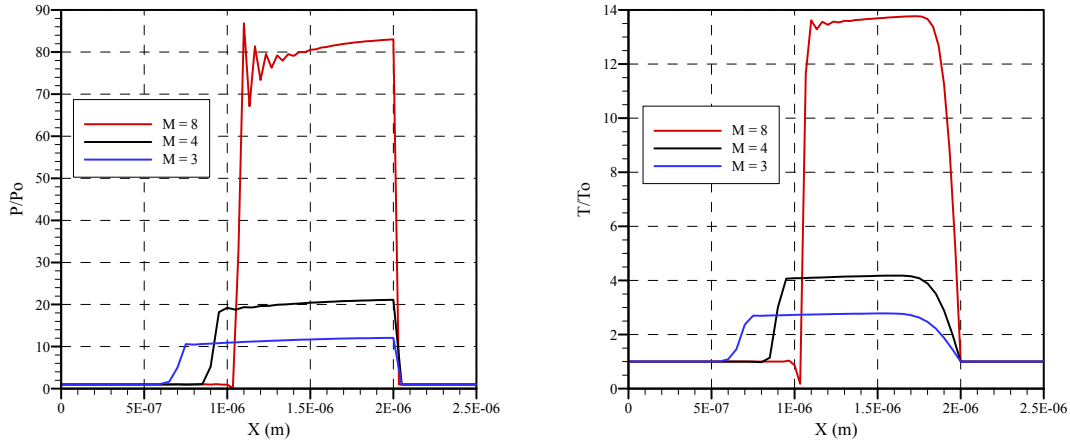

a) *b*)

Figure 6. Pressure and Temperature profiles along the Obstacle's midplane.

From Figures 6 *a*) and *b*), one can observe that, as the Mach number increases, the shock thickness decreases, causing even oscillations in the pressure and temperature across the shock for Mach number 8. Also, the detachment distance of the shock from the tip of the obstacle decreases as Mach number increases, *i.e.*, the shock gets closer to the obstacle.

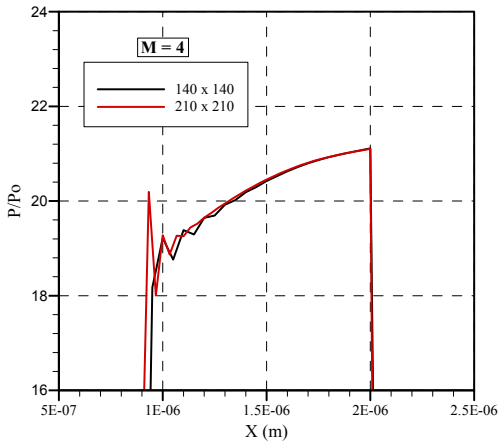

Figure 7. Influence of the mesh on the shock capturing and resolution.

From Fig. 7 one can notice the influence of the mesh size on the shock capturing through the oscillations that appear in the pressure (and temperature) profile. As the mesh is refined for the higher Mach numbers, the shock position is captured more accurately, causing a quicker damping of the oscillations. This happens because the shock thickness decreases with increasing Mach number, becoming very thin for high Mach numbers, consequently demanding more refined meshes. This, in turn, makes computational efforts more demanding.

Finally, Fig. 8 *a*) and *b*) show the contour maps for the temperature and pressure for Mach number 8. As can be seen, there is a strong expansion inside the shock on the obstacle's sidewall. The temperature remains relatively high while the pressure almost reaches the free stream value after a compression of about 80 times the free stream pressure.

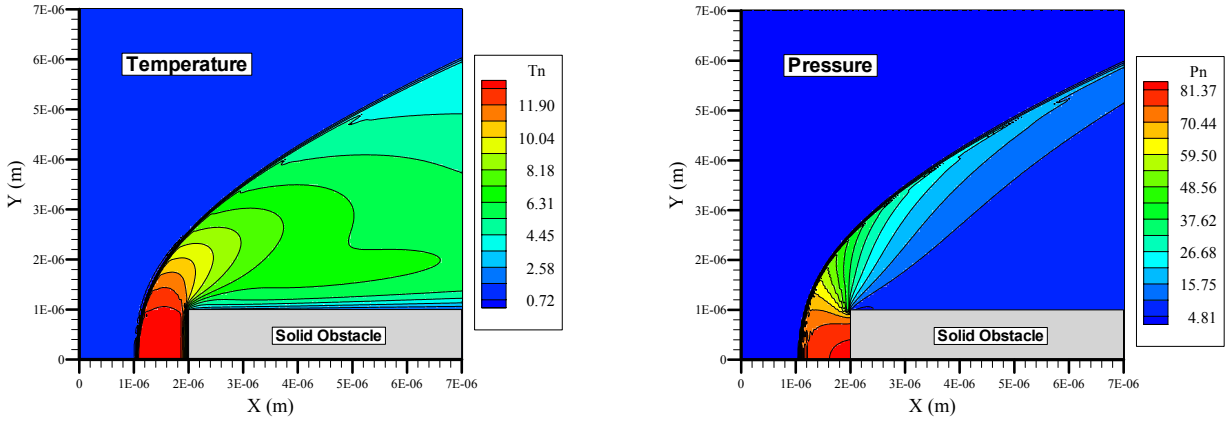

a) *b*)

Figure 8. Pressure and Temperature contours for Mach number 8.

Table 2 shows the values of the pressure and temperature ratios behind and in front of the shock, for the normal shock relations shown at, *e.g.*, Anderson (1990). As can be seen, the results compare very well with the ones shown in Fig. 6 *a*) and *b*).

Table 2. Pressure and Temperature ratios for the Normal Shock relations.

	p_2/p_1			T_2/T_1		
Mach number	3	4	8	3	4	8
Normal Shock relations	10.33	18.50	74.50	2.68	4.05	13.39

6. Conclusions

In this work the high speed flow over a flat plate and on a step obstacle were investigated from a numerical point of view. The MacCormack's time marching technique was used to solve the flow equations. The results presented show some interesting numerical and physical aspects of these two distinct types of shock waves, although the fluid was considered as a calorically perfect gas. The results compared well with the ones found in the literature. As a next step in this research line, the utilization of real gas properties is being planed in order to make the results more realistic.

7. Acknowledgements

The authors wish to express their acknowledgement to FAPESP (project N^{o} 03/06888-1 and project N^{o} 04/00525-7) and AEB for partially supporting this work.

8. References

Anderson, J. D. Jr., 1989, "Hypersonic and High Temperature Gas Dynamics", McGraw Hill, US.

Anderson, J. D. Jr., 1990, "Modern Compressible Flow - With Historical Perspective", McGraw Hill, Singapore.

Anderson, J. D. Jr., 1995, "Computational Fluid Dynamics", McGraw Hill, New York.

Moraes, A. C. M.; Flaherty, J. E.; Nagamatsu, H. T., 1991, "A Study of Compressible Laminar Boundary Layers at Mach Numbers 4 to 30", AIAA 91-0323, *29th Aerospace Sciences Meeting*.

Nagamatsu, H. T.; Messit, D. G.; Myrabo, L. N.; Sheer, R. E. Jr., 1994, "Computational, Theoretical and Experimental Inventisgation of Flow over a Sharp Flat Plate M_1 10-25", AIAA 94-2350, *25th AIAA Fluid Dynamics Conference*.

Toro, P. G. P.; Rusak, Z.; Myrabo, L. N. and Nagamatsu, H. T., 1998, "Hypersonic Flow over a Flat Plate", AIAA 98-0683.

"LEVSOFT: A Software Platform for 2D Computer Aided Engineering", 1998, http://www.lev.ieav.cta.br.

9. Responsibility notice

The author(s) is (are) the only responsible for the printed material included in this paper.